Direct Comparison of the Submicron Aerosol Hygroscopicity of Water-Soluble Sugars

Joseph Nelson Dawson[1], Kotiba A. Malek[2], Patricia N. Razafindrambinina[3], Timothy M. Raymond[2], Dabrina D Dutcher[2,4*], Akua Asa-Awuku[3,5*], and Miriam Arak Freedman[1*]*

[1]Department of Chemistry, The Pennsylvania State University, University Park, PA 16802, United States of America

[2]Department of Chemical Engineering, Bucknell University, Lewisburg, PA 17837, United States of America

[3]Department of Chemistry and Biochemistry, University of Maryland, College Park, MD 20742, United States of America

[4]Department of Chemistry, Bucknell University, Lewisburg, PA 17837, United States of America

[5]Department of Chemical and Biomolecular Engineering, University of Maryland, College Park, MD 20742, United States of America

*Correspondence: Miriam Arak Freedman (maf43@psu.edu); Akua Asa-Awuku (asaawuku@umd.edu); Dabrina D Dutcher (ddd014@bucknell.edu); Timothy M. Raymond (traymond@bucknell.edu)

KEYWORDS: hygroscopicity, optical growth factor, water-soluble, organic aerosol, Cloud Condensation Nuclei, sucrose, levoglucosan

ABSTRACT

Water-soluble organic compounds (WSOCs) readily uptake water and form atmospheric droplets. Understanding the water uptake ability of these WSOCs can improve our understanding of their radiative effects, and thus can improve current climate models. In this study, we measure the subsaturated and supersaturated droplet growth of four WSOCs: levoglucosan, sucrose, raffinose, and trehalose. Specifically, we use three distinct nanoscale droplet growth methods: cavity ring-down spectroscopy (CRDS), hygroscopic tandem differential mobility analysis (H-TDMA), and cloud condensation nuclei (CCN) counting; and report optical growth factor (*f*RH), growth factor (G_f), refractive indices, and critical activation diameters (d_{p50}) for each aerosol system. Ideal thermodynamic Köhler theory is applied, and the single parameter hygroscopicity, κ, is reported for the four WSOCs. Additionally, we compare two methods for calculating the κ-values from *f*RH data. Results are compared to droplet activation theory and hygroscopicity parameterizations and discussed within the context of current findings in the literature. We show that the single parameter hygroscopicity term for water-soluble sugars is dependent on molecular weight, in agreement with Köhler theory for compounds with similar densities. The three experimental methods have comparable precision with systematic deviations in the average mean for each method. Better hygroscopicity comparisons can be made with literature values by understanding the relationship between the κ-values obtained via different techniques. Understanding the hygroscopicity of these saccharides in the sub- and supersaturated regimes using several different techniques can help us understand the water uptake properties of non-surface active WSOCs in atmospheric systems.

1. INTRODUCTION

Aerosol particles affect the radiative budget of the Earth through their interactions with solar radiation. Specifically, aerosol particles influence the radiative budget via direct and indirect effects. The direct effect results from the scattering or absorption of light by the particles themselves.[1] In addition, many aerosol particles are hygroscopic; and, therefore, may act as cloud condensation nuclei (CCN), taking up water and leading to the formation of droplets and clouds; this interaction is known as the indirect effect. Changes in the amount of water adsorbed subsequently affect the scattering and absorption of light. Thus, the ability of water to condense and partition from gas to liquid on particle surfaces has significant implications for visibility, air quality, and climate. [2,3]

Organic aerosols are ubiquitous in the atmosphere; however, their interactions with water (water-uptake, diffusivity, etc.) are poorly understood.[4] Specifically, water-soluble organic compounds (WSOCs) make up a significant fraction of the organic composition and are emitted by large aerosol sources such as biogenic and biomass burning sources.[5–9] WSOCs with solubilities above 100 g L^{-1} are assumed to fully dissolve and readily uptake water.[10,11] However, solubility does not fully describe hygroscopicity and, thus, understanding other chemical and physical properties of WSOCs (e.g., structure, molecular weight, density) are critical to predicting particle water uptake.

In this work, we measure droplet growth of four WSOCs: levoglucosan, an anhydrosugar, and three disaccharides (sucrose, raffinose, trehalose). Levoglucosan is one of the most abundant atmospheric carbohydrates and is a well-studied marker of biomass burning.[12–14] The ability of levoglucosan to promote atmospheric droplet formation has been measured with different techniques. Rosenørn et al.[15] used a static-thermal gradient type cloud condensation nuclei counter (CCNC) and Svenningsson et al.[16] used a hygroscopic tandem differential mobility

analyzer (H-TDMA) and CCNC to measure the droplet growth of levoglucosan particles in sub- and supersaturated environments.[15,16] Water-uptake behavior has been measured for levoglucosan with an electrodynamic balance (EDB); however, these experiments deal with micron-sized particles, unlike the methods used in this work, which investigate the much smaller submicron aerosol particles.[17,18] Lei et al. .[19], Mochida and Kawamura[20], and Svenningsson et al. .[16] all observed no deliquescence phase transition for levoglucosan below 100% relative humidity (R.H.). Levoglucosan particles retained water as low as 5% RH.[16,19,20]

In addition to levoglucosan, three sugars (sucrose, raffinose, and trehalose) are studied. Sucrose, though less atmospherically prevalent than levoglucosan, has been measured in ambient aerosols and is also thought to be a good proxy for highly soluble and viscous WSOCs.[21–23] The ability of highly viscous "glassy" sucrose nanoparticles to uptake water is of recent interest and has been well studied.[24–32] Furthermore, Koop et al. .[33] published that the glass transition temperature, the relative magnitude of which indicates the relative amount of hygroscopic growth, depends strongly on molecular weight more than functional groups or O:C ratio.[33] Rosenørn et al. .[15] measured the CCN activity of sucrose and other saccharides and identified differences in molecular weight as a source of significant change in hygroscopicity.[15] Lee et al. .[34] took H-TDMA measurements of sucrose to compare atomic force microscopy techniques to other viscosity measurements.[34] Hence, we probed the water uptake of two additional sugars with higher molecular weight than sucrose (raffinose and trehalose, Table 1). Trehalose is atmospherically relevant and can be used as a marker for biogenic secondary organic aerosol (SOA) or biologically active surface soils.[35,36] Raffinose is an oligosaccharide with higher molecular weight and lower solubility (Table 1). Sucrose, raffinose, and trehalose have been recently identified as amorphous particles in the subsaturated regime.[30] To our knowledge,

CCNC and H-TDMA measurements have not been conducted for raffinose or trehalose although some work with the water uptake of particles > 1 μm has been performed.[30]

Table 1. Information for Each Water Soluble Organic Compounds with Calculated Refractive Indicies

	Structure	Molecular Weight [g mol^{-1}]	Solubility @ 298 K [g L^{-1}]	Density [g mL^{-1}]	O:C	RI_{exp}	κ Ideal
Levoglucosan		162.1	62.3[a]	1.7[b]	0.833	1.550 ± 0.006	0.190
Trehalose	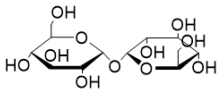	342.3	689[c]	1.58[d]	0.917	1.495 ± 0.005	0.083
Sucrose	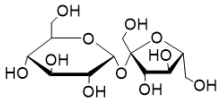	342.3	2040[d]	1.59[d]	0.917	1.510 ± 0.012	0.084
Raffinose	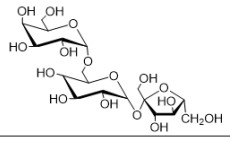	504.4	143[d]	1.465[d]	0.889	1.492 ± 0.016	0.064

A recent article has summarized the available experimental techniques for hygroscopicity measurements, including techniques for micron-sized particles such as EDB.[37] While several submicron WSOCs hygroscopicity measurements have been conducted with H-TDMA or CCNC, fewer studies report optical growth factor (*f*RH).[38–41] Optical growth factor measurements of laboratory WSOCs are rare in the literature, and much of the hygroscopicity data of levoglucosan, sucrose, raffinose, and trehalose has been obtained with H-TDMA. But measurements of optical growth factors are important because they provide a direct measure of how light interacts with particles, rather than extrapolating the effects of light using geometric growth factors. To our knowledge, only two studies have measured the *f*RH of levoglucosan, and only one study has measured *f*RH for sucrose and raffinose.[39,42,43] Traditionally, cavity ring-down spectroscopy (CRDS) has been used to measure gas-phase spectra and, more recently,

was developed to measure the extinction of light by small particles.[44] In this work, we used two cavities in series to measure the water uptake of the WSOCs. Unlike H-TDMA, which measures a geometric growth factor (G_f) based on particle size, CRDS measures an optical growth factor (fRH) based on light scattering and absorption. Therefore, CRDS provides intrinsic optical data in addition to water uptake data.

In the work cited above, rarely are more than two droplet growth measurements simultaneously published. Taking more than one type of measurement is helpful to span sub- and supersaturated regimes as well as to investigate the differences between techniques. Only one study, Wex et al. .[45] used an optical particle spectrometer (OPS) with H-TDMA and CCNC measurements to study the hygroscopic growth of α-pinene SOA.[45] In this paper, droplet growth (on the nanoscale) is measured in the sub-saturated relative humidity regime with both a CRDS and a H-TDMA as well as being measured in the supersaturated regime with a CCNC. Using these data, the single-parameter hygroscopicity (κ) was calculated from all three methods and compared with one other method of converting fRH to κ.[46] Intercomparisons of different methods are important to investigate the differences and similarities between techniques and to gain insight into fundamental processes.

In summary, in this paper, we have measured the water uptake of four WSOCs, levoglucosan, raffinose, sucrose, and trehalose, using three techniques, CRDS, H-TDMA, and CCNC. Through use of these three techniques, we have measured water uptake under subsaturated and supersaturated conditions. To compare the different methods, we have converted all of our measured data to a single-parameter hygroscopicity (κ) value. Our goals are to compare the hygroscopicity of these WSOCs measured with these different techniques over the sub- and

supersaturated regimes in order to both gain insight into the hygroscopicity of WSOCs and these techniques.

2. Experimental Methods

The ability of a submicron particle to uptake water and form a droplet was estimated via optical growth factor (*f*RH), geometric growth factor (G_f), and supersaturated (CCN activity) measurements. Each experimental setup was calibrated with ammonium sulfate aerosol. Ammonium sulfate and each of the four WSOCs aerosols was generated from bulk solutions using a constant output atomizer (TSI 3076) (Fig. 1). A dilute solution (0.1 wt% – 0.8 wt%) of the analyte was formed by dissolving the commercially obtained chemical (ammonium sulfate, 98%, Millipore™; sucrose, 99% Fisher Chemical™; D(+)-raffinose (pentahydrate), 97%, Dot Scientific Inc.™; D-trehalose (di-hydrate), 99%, Sigma-Aldrich™; 1,6-anhydro-beta-d-glucopyranose (levoglucosan), 99%, ACROS Organics™) in ultrapure water (high-performance liquid chromatography grade or Millipore(R) Water >18 MΩ). The solution was then atomized by a 3.6 L min^{-1} carrier gas of medical air (purified air with H_2O < 67 ppmv) that underwent further purification with a Speedaire oil coalescing filter, a Speedaire particulate filter, activated carbon filter, and two HEPA filters to remove particulate matter and trace gases. Subsequently, the aerosol particles were dehydrated through the use of a diffusion dryer filled with silica gel such that particles were dry (< 10% R.H.) when exiting the diffusion dryer.[47] Specifically, the removal rate (which has previously been measured) was 98% R.H. sec^{-1}.[47] The dry aerosol flow was split to the separate systems and measured for optical growth, geometric growth, and CCN activity (Fig. 1). The sections below briefly describe the methods and calculations presented in this study. The three experimental methods can be directly compared

with the calculation of a single-hygroscopicity parameter derived from Köhler theory (Sect. 3). The sections below briefly describe the methods and calculations presented in this study.

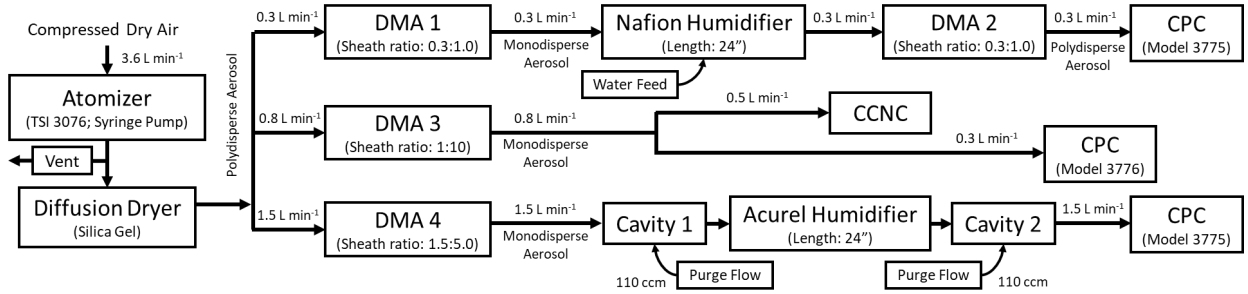

2.1 Cavity Ring-Down Measurements

Each of the four WSOCs was atomized and dried, as described above (Sect. 2). The dried particles were then analyzed using cavity ring-down spectroscopy. The cavity ring-down system consists of a few key components previously described and only briefly covered here.[48–50] A 643 nm continuous-wave diode laser (Power Technologies) was modulated at 500 Hz and was coupled to two 91 cm long cavities. The cavities were capped at both ends with highly reflective mirrors (> 99.9985% reflective @ 640 nm; ATFilms, Boulder, CO) such that each cavity had an effective path length of approximately 48 km. The light transmitted through the CRDS cavity was measured by a photomultiplier tube. The first-order decay constant fitted to the decay of light is known as the ring-down time, τ. Extinction coefficients (α_{ext}) were then calculated using Eq. (1) from the ring-down times within the cavity

$$\alpha_{ext} = \frac{R_L}{c}\left(\frac{1}{\tau} - \frac{1}{\tau_0}\right), \quad (1)$$

where R_L is the ratio of cavity length to the length of the cavity that the sample occupies, c is the speed of light, and τ, τ_0 are the ring-down times (first-order decay constants) with and without sample, respectively..[51] A purge flow (55 sccm) was maintained across each mirror to prevent

dust or sample from accumulating on them. This flow rate diluted the sample to a known degree, which is accounted for using simple dilution calculations when determining particle concentrations. The laser was pulsed while the purified air flowed through the cavity at a rate of 1.5 L min^{-1}. The background ring-down time was established when no aerosol sample was present in the cavity. An aerosol sample was dried by the diffusion dryer and then size selected with an electrostatic classifier (TSI 3080) and a differential mobility analyzer (DMA, TSI 3081) maintaining an aerosol to sheath flow of 1.5:5.0. This DMA is optimized for an aerosol to sheath flow of 1:10. That this ratio is smaller than 1:10 results in a broader transfer function. We have used a ratio of 1.5:5.0 for CRDS to keep the sheath flow constant over the range of sizes characterized. The sample was then directed into the cavity to obtain the extinction coefficient of the sample. After passing through the cavity, particles were sampled by the condensation particle counter (CPC, TSI 3775) where particle concentration was obtained.

2.1.1 Refractive Index Measurement

Once the extinction coefficients and the particle concentrations were obtained, the extinction coefficients, determined from each laser shot, were averaged to determine the average extinction coefficient for each selected size. Simultaneously, the concentration of particles was monitored and subsequently averaged. Due to the purge flow within each cavity of the CRDS, the concentration of particles was minimally diluted. Using the known flow rates of both the experiment and the purge flow, the concentration of particles was corrected to account for the purge flow. It should be noted that particles selected by the DMA can be multiply charged. For this reason, we corrected the experimental data for these multiply charged particles as described by Freedman et al.[52] The extinction cross-section (σ) was calculated by Eq. (2) from the experimentally determined values as follows

$$\sigma_{exp} = \frac{\alpha_{exp,avg}}{N_{avg}},$$

(2)

where $\alpha_{exp,ave}$ is the average extinction coefficient, and N_{avg} is the averaged particle concentration . Extinction cross-section is related to extinction efficiency, Q_{ext} by

$$Q_{ext} = \frac{\sigma_{ext}}{\pi r^2}, \quad (3)$$

where r is the particle radius. Theoretical extinction efficiencies for a range of refractive index values are calculated using Mie theory, converted to extinction efficiencies using Eqs (2) and (3), and compared with the experimental values to determine the refractive index value with the best fit to the experimental data. The best fit is calculated using the cumulative fractional difference (CFD_R)

$$CFD_R = \frac{1}{P} \sum_{AllSizes} \frac{\left|\alpha_{ext,ave} - \alpha_{ext,Mie}\right|}{\alpha_{ext,ave}}, \quad (4)$$

where $\alpha_{exp,Mie}$ is the theoretical extinction efficiency, and P is the number of particle sizes selected. The best fit refractive index is that which has the lowest CFD_R.[52,53]

2.1.2 Optical Growth Measurement

The dual cavity CRDS system is shown in Fig. 1. In this system, two CRDS cavities were connected in series with a custom-built humidifier (Membrane: Accurel V8/2) between them. The background ring-down time was measured for both cavities as for the refractive index calculations. Size selected dried aerosol particles (< 10% R.H.) were then drawn through the first cavity at 1.5 L min^{-1}. The extinction of light by the introduction of the dry particles into the first cavity was measured. Then the particles passed through the humidifier where the relative humidity of the particles was increased to 85% ± 3%. The extinction of light by the humidified particles was then measured in the second cavity before the concentration of particles was

measured by the condensation particle counter (TSI 3775). Eq. (5) expresses that the optical growth factor (*f*RH) is calculated, in this work, by dividing the extinction cross-section of the humidified particles ($\sigma_{ext,a}$) by the extinction cross-section of the dry particles ($\sigma_{ext,b}$)

$$fRH(a,\ b) = \frac{\sigma_{ext,a}}{\sigma_{ext,b}}, \quad (5)$$

where *a* is the relative humidity of the humidified particles, and *b* is the relative humidity of the dry particles (<10 % R.H.)[42]. The *f*RH was determined for each compound at seven different sizes (200 nm through 500 nm with a 50 nm interval) and then averaged together for a single value. Note that in contrast to the measurement of optical properties, these measurements are not corrected for the presence of multiply charged particles because we do not know the diameter of the wet particles.

2.2 Humidified Tandem Differential Mobility Analysis Measurements

A humidified tandem differential mobility analyzer (H-TDMA) was used to measure the subsaturated growth factor of ammonium sulfate and the WSOCs. The H-TDMA is widely used for aerosol hygroscopic measurement, and a detailed setup has been previously described (Fig. 1) (e.g., but not limited to Refs. [54–57]). The dry aerosol was size selected with an electrostatic classifier (TSI 3081) at three particle electrical mobility diameters; 200, 250, and 300 nm. The aerosol flow rate was 0.3 L $min^{-1,}$ and the sheath flow was 1.0 L min^{-1}. The size selected particles were then humidified up to 95% R.H. with a Nafion humidification line (PermaPure® M.H. series). The size distribution and concentration of the humidified particles were subsequently measured with a second, RH equilibrated DMA (TSI 3081) and a condensation particle counter (TSI 3775) (Fig. 1 and Fig. S1). The DMA was equilibrated by exposure to constant R.H. until both the inlet and outlet flow of the DMA reached the same R.H.

2.3 Cloud Condensation Nuclei Measurements

The critical activation diameters (d_{p50}) of ammonium sulfate and the four WSOCs were measured at varying supersaturations. The dry aerosol size distributions were measured with a scanning mobility particle sizer (SMPS, TSI 3081) and a condensation particle counter (TSI 3776). A cloud condensation nuclei counter (CCNC; Droplet Measurement Technologies, DMT ©) was operated downstream of the SMPS in parallel with the CPC. The CCNC sampled the size-selected aerosol at 0.5 L min^{-1} flowrate. The activated fraction, the CCN concentration divided by the aerosol number concentration, was measured between supersaturations of 0.3 – 1.2% for different particle dry diameters. Scanning mobility CCN analysis (SMCA) was employed and used to calculate the critical activation diameters for each supersaturation.[58] A multiple charge correction is applied with SMCA, and a sigmoid is fit through the data, neglecting the charged particles.[58] The CCNC was calibrated with $(NH_4)_2SO_4$ aerosol to determine the instrument R.H. (Fig. S5). The calibration of $(NH_4)_2SO_4$ aerosol requires the estimation of water activity.[59–62] The method used for instrument calibration assumes a van't hoff factor equal to 2.5.[59]

Initially, dry particles were also size selected with an SMPS for CCN measurement.[63] Each scanned size distribution scan was 135 seconds, and the SMPS sheath to aerosol flow was set to 10:1. After size selection, the monodisperse particle stream was split. A condensation particle counter (TSI 3776) sampled at a rate of 1.5 L min^{-1} and provided total particle concentration information. The second stream was drawn by a continuous flow streamwise thermal gradient DMT CCNC at a rate of 0.5 L min^{-1}.

2.4 Hygroscopicity Analysis

The equilibrium vapor pressure at the surface of a droplet was calculated by Eq. (6) as a function of the ambient relative humidity

$$\frac{RH}{100} = a_w exp\left(\frac{4\sigma_{s/a} M_w}{RT\rho_w D_{dry}}\right), \quad (6)$$

where, a_w is the water activity of the droplet, $\sigma_{s/a}$ is the surface tension of the droplet at the air droplet interface, R is the universal gas constant, T is the temperature of the droplet, M_w and ρ_w are the molecular weight and density of water, respectively, and D_{dry} is the dry particle diameter.[46] By rearranging Eq. (6) and assuming that the solute is sufficiently dilute in the droplet, a_w can be simply defined with a single parameterization

$$\frac{1}{a_w} = 1 + \kappa\frac{V_{dry}}{V_{wet}}, \quad (7)$$

where V_{dry} and V_{wet} are the volumes of the dry and wet particle, respectively, and κ represents a single hygroscopicity parameter reflective of the aerosol chemical composition, which is described in more detail below.[46] The parametrization by Petters and Kreidenweis[46] suggests that κ can be calculated at both subsaturated and supersaturated conditions. Kreidenweis and Asa-Awuku[64] and the references therein provide a full derivation of κ under both conditions.[64,65] Briefly, if the wet and dry particles are assumed to be spherical, then volume can be converted to particle diameter, D, and the growth factor, G_f, as defined by Eq. (8) can be calculated

$$G_f(a, b) = \frac{D_{wet}}{D_{dry}}, \quad (8)$$

where the diameter of the humidified particle (D_{wet}) is divided by the diameter of the dry particle (D_{dry}). At high relative humidities (>85%), the vapor pressure of water approaches that of a flat surface (the Kelvin effect is negligible for surfaces over 200 nm diameters), and the a_w can be approximated with R.H. Thus, G_f is simplified to Eq. (9) as follows:

$$G_f^{\ 3} = 1 + \kappa\left(\frac{RH/100}{1-RH/100}\right). \quad (9)$$

[46,64]For supersaturated CCN measurement, κ is calculated via

$$\kappa = \frac{4\left(\frac{4\sigma_{s/a} M_w}{RT\rho_w}\right)^3}{27 D_{dry}^3 ln^2 s_c} \quad , \quad (10)$$

where s is the instrument supersaturation, and the critical dry diameter is substituted for d_{p50}.[46,64,65] Unlike for H-TDMA and CCNC measurements, the equations for single hygroscopicity optical growth measurements, fRH, have not been explicitly derived. Previous studies have proposed two and three empirical parameter relationships between fRH and RH.[40,42,64] Currently, two techniques are available to obtain a single hygroscopicity parameter and are described below.

In the first method, the optical growth factor was converted to geometric growth factor using Mie theory and the experimentally derived refractive indices. The mobility diameter of the dry aerosol particles was selected with the DMA. However, the diameter of the humidified particles was calculated by extrapolating the water content of the humidified particle from the optical growth factor calculation and Mie theory. First, the volume-weighted refractive index (m_t) is calculated

$$m_t = \sum_i \frac{V_i}{V_t} m_i, \quad (11)$$

using the real part of the refractive index of the sample that is experimentally determined, as shown in Eq. (11). The real part of the refractive index of water at 643 nm was obtained from Lavallard et al. .[66] where V_i is the volume of the component i and m_i is the real part of the refractive index of component i.[66] Only the real part of the refractive index was used since the absorption of these compounds is negligible at 643 nm. Extinction coefficients were calculated

for every particle size 0.1 nm above the dry particle diameter to obtain an extinction coefficient for comparison of the experimentally determined optical growth factor. The diameter that resulted in minimum variation between the calculated optical growth factor and the experimentally obtained optical growth factor was used to calculate geometric growth factor using Eq. (8).[4] Eq. (12) is used to derive the κ value from the growth factor

$$\kappa = (G_f^{\,3} - 1)\left[\frac{100}{RH} e^{\left(\frac{4\sigma_{s/a} M_w}{RT\rho_w D_{dry} G_f}\right)} - 1\right], \quad (12)$$

where $\sigma_{s/a}$ is the surface tension between the solution and the air, assumed to be that of water; ρ_w is the density of water, M_w is the molecular weight of water, R is the gas constant, and T is the standard temperature[64]. These assumptions are often used for supersaturated κ calculations, where the water content of the aerosol particles is very high but might be less than ideal for the calculation of subsaturated κ values.

In addition to the above method for calculating κ value, another empirical method has been proposed. This semi-empirical derivation is found in Kreidenweis and Asa-Awuku[64]. In Kreidenweis and Asa-Awuku[64], the geometric growth factor is related to optical growth factor via the following empirical relation and is shown here in Eq (13),

$$fRH(80\%RH,\ dry) = G_f(80\%RH,\ dry)^{\left(\frac{0.86}{0.28}\right)}. \quad (13)$$

[64]Using Eq. (9) in conjunction with Eq. (13) the following semi-empirical relation of Eq. (14) is derived

$$\kappa_{Empirical} = \left(fRH(80\%RH,\ dry)^{\frac{3*0.28}{0.86}} - 1\right)\left(\frac{1-RH/100}{RH/100}\right). \quad (14)$$

In Kreidenweis and Asa-Awuku[64], the empirical correlation between growth factor and optical growth factor was determined on systems conducted at 80% R.H. with limited experimental data.

Here the distinction is made between optical growth κ values determined by Mie theory and those determined semi-empirically as $\kappa_{CRD,Mie}$ and $\kappa_{CRD,Empirical,}$ respectively.

3. Results and Discussion

*3.1 Optical Growth Factors, f*RH

Optical growth factors and refractive indices were determined for each of the WSOCs: levoglucosan, trehalose, sucrose, and raffinose. The refractive indices are displayed in Table 1 and Supplemental Fig. S2. Supplemental Fig. S3 shows a representative plot for the optical growth factor of ammonium sulfate at 84.4% ± 2.7% R.H., as determined by CRDS with a 643 nm laser. These results show good agreement when compared to Mie theory using 85% R.H. That the data lie above the theory line is consistent with the literature[39,42], and is due to the inclusion of multiply charged particles in the calculation of *f*RH. Our standard deviation between measurements is slightly higher than reported previously due to the higher R.H. of our measurements (~85% compared with ~80%). Because ammonium sulfate is highly hygroscopic, subsaturated growth is extremely sensitive to changes in R.H., and this sensitivity increases as the R.H. increases. We would, therefore, expect measurements conducted at higher R.H. to have more error. The *fRH* data for each of the compounds are displayed in Fig. 2. When compared to previous studies, our values are consistently higher, which is likely the result of higher relative humidity in our experiment, as described in detail below. Our study found that for levoglucosan, the *f*RH (82.4% R.H., dry) was 2.32 ± 0.18 at an effective diameter of 250 nm, and the *f*RH (83.3% R.H., dry) was 1.65 ± 0.14 at an effective diameter of 500 nm. For the same system but at different relative humidity, Garland et al.[42] found an *f*RH (80% R.H., dry) of 1.71 ± 0.05 at an effective diameter of 254 nm and an *f*RH (80% R.H., dry) of 1.47 ± 0.04 at an effective diameter

of 532 nm. Our study is performed with a 643 nm laser while Garland et al.[42] used a 532 nm laser. In addition, measurements of water uptake are extremely sensitive to the R.H. of the experiment. In our study, the *f*RH (85.8% R.H., dry) is 1.79 ± 0.22 for sucrose, and the *f*RH (88.0% R.H., dry) is 1.83 ± 0.18 for raffinose. In a different study, Robinson et al.[43] determined the optical growth factor *f*RH (80% R.H., dry) was 1.24 for sucrose and 1.25 for raffinose.[43] Like Garland et al.[42], Robinson et al.[43] used a 532 nm laser for their study. Optical growth factors are shown in Fig. 2 for each of the four WSOCs measured here. The *f*RH decreases with increasing dry particle size, which is consistent with prior *f*RH studies.[39,42] The decrease in *f*RH with particle size is due to the fact that extinction cross-sections increase non-linearly with particle diameter, with the steepest increase at the smallest diameters.[52] Thus, the same amount of geometric growth will result in a larger measured *f*RH for a smaller particle than a larger one. Since *f*RH is strongly dependent on R.H., small changes (~5%) in R.H. can significantly modify *f*RH values. For direct comparison of optical growth, differences in R.H. must be considered. The conversion to κ-values (as shown in Section 3.4) allows for direct comparison. Raffinose has similar *f*RH values as sucrose but was measured at higher R.H., meaning that, if the data were normalized for R.H., it would have the lowest *f*RH values.

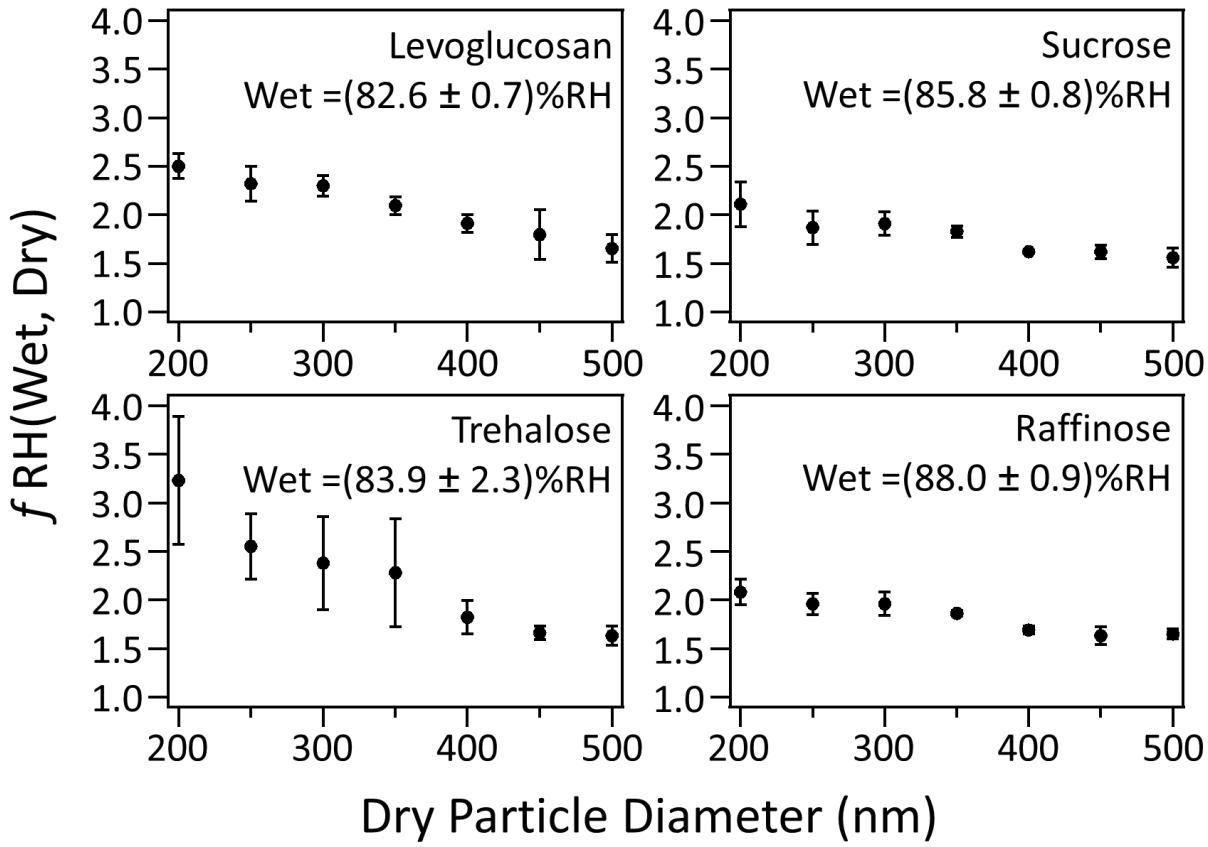

Table SEQ Table * ARABIC 2. Average Measured and Calculated Values for Each of the Water-Soluble Organic Compounds

	fRH (%RH)	$G_{f,fRH}$ (%RH)	$G_{f,HTDMA}$ (%RH)	κ_{ideal}	κ_{Mie}	$\kappa_{empirical}$	κ_{HTDMA}	κ_{CCNC}
Levoglucosan	2.08 ± 0.32 (82.6%)*	1.31 ± 0.01 (82.6%)*	1.64 ± 0.09 (95%)	0.190	0.277 ± 0.055	0.221 ± 0.066	0.180 ± 0.038	0.21 ± 0.03
Trehalose	2.22 ± 0.64 (83.9%)*	1.29 ± 0.03 (83.9%)*	1.33 ± 0.01 (95%)	0.083	0.221 ± 0.049	0.214 ± 0.089	0.071 ± 0.003	0.11 ± 0.02
Sucrose	1.79 ± 0.22 (85.8%)*	1.23 ± 0.01 (85.8%)*	1.41 ± 0.02 (95%)	0.084	0.144 ± 0.024	0.127 ± 0.041	0.096 ± 0.008	0.12 ± 0.02
Raffinose	2.01 ± 0.44 (88.0%)*	1.22 ± 0.01 (88.0%)*	1.20 ± 0.04 (95%)	0.064	0.117 ± 0.015	0.109 ± 0.020	0.039 ± 0.010	0.07 ± 0.01

*Note: The relative humidity used in these calculations have an associated error for each calculation. These values are found in the body of the text.

3.2 H-TDMA Growth Factors, G_f

Geometric growth factors were determined for each of the WSOCs at three dry particle diameters, and the average growth factor for each compound is shown in Table 2. The growth

factors determined in this study agree with the growth factors calculated from the theoretical κ value well across the measured particle sizes (Fig. 3, Eq. 9). Trehalose and raffinose are not well studied and, to the best of our knowledge, do not have previously reported H-TDMA growth factors. H-TDMA growth factors are also R.H. dependent, and the reported values are consistent with previously reported data measured at a different R.H. as higher saturation leads to larger geometric droplet growth. The geometric growth factor for levoglucosan at 95% R.H. was 1.64 ± 0.09. Svenningsson et al.[16] reported the levoglucosan growth factor to be approximately 1.59 at the same conditions. (Please note that all literature data for all techniques are compared and plotted in Section 3.4 below.) Using an R.H. of 90%, Koehler et al.[67] reported two smaller values for growth factor using H-TDMA, approximately 1.36 and 1.39. The study with values closest to this study was performed by Chan et al. .[17] with an electrodynamic balance and found the growth factor to be approximately 1.6 at 96% R.H. Similar to Koehler et al.[67], Mochida and Kawamura[20] did not measure growth factor at 95% R.H., but at 90% R.H., the geometric growth factor of levoglucosan was 1.38.[20] Our work had determined the growth factor of sucrose with 200 – 300 nm dry diameters to be 1.41 ± 0.02 at 95% RH.[3131 Tong et al. .31] measured the growth factor of sucrose to be ~1.19 at 80% R.H. using optical tweezers on supermicron particles at a significantly lower R.H. than our study. It should be additionally noted that the particles in Tong et al.[31] had micrometer diameters. Hodas et al.[27] found the growth factor of sucrose to be ~1.25 at 90% using a differential aerosol sizing and hygroscopicity spectrometer probe (DASH-SP). H-TDMA was also used by Estillore et al.[26] to determine the geometric growth factor of sucrose at 90% R.H. and was found to be about 1.24 using similar particle generation with sizes likely similar to those presented here.[26]

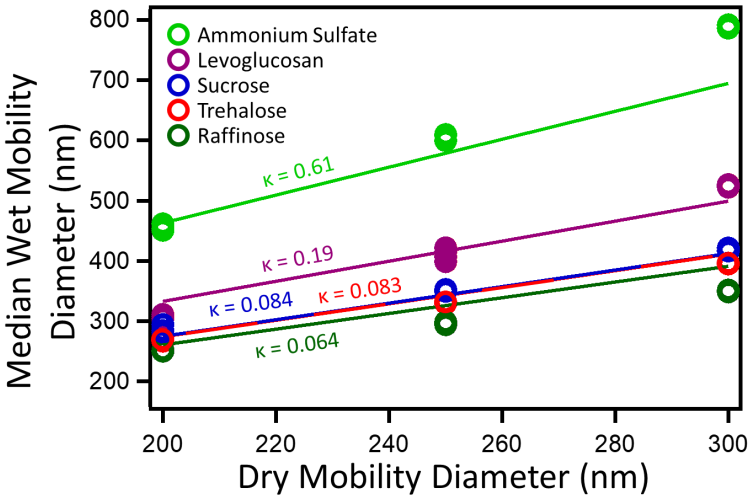

3.3 CCN Activation Results: CCN Activity

The critical diameters (d_{p50}) were measured for each of the WSOCs and ammonium sulfate at varying instrument supersaturation, and initial R.H. Figure 4a shows exemplary sucrose CCN activation data measured at 0.5 L min^{-1} under dry aerosol initial conditions. The d_{p50} increases with decreasing instrument supersaturation, and κ-values remain constant over the range of instrument supersaturation (0.12 ± 0.02, Table 2). The measured κ_{CCNC} for all four WSOCs is slightly larger but within the uncertainty of ideal values. Sucrose is known to increase droplet surface tension (Supplemental Information Fig. S4).[34] However, at the measured aerosol concentrations, the impact of surface tension on the droplet is negligible in this case. For small (40 nm) and large critical diameters (250 nm), the calculated hygroscopicity (accounting for changes in $\sigma_{s/a}$) remains 0.084 (Fig. 4b). Accounting for changes in surface tension does not reasonably explain the higher measured WSOCs κ_{CCNC} values shown in Table 2.

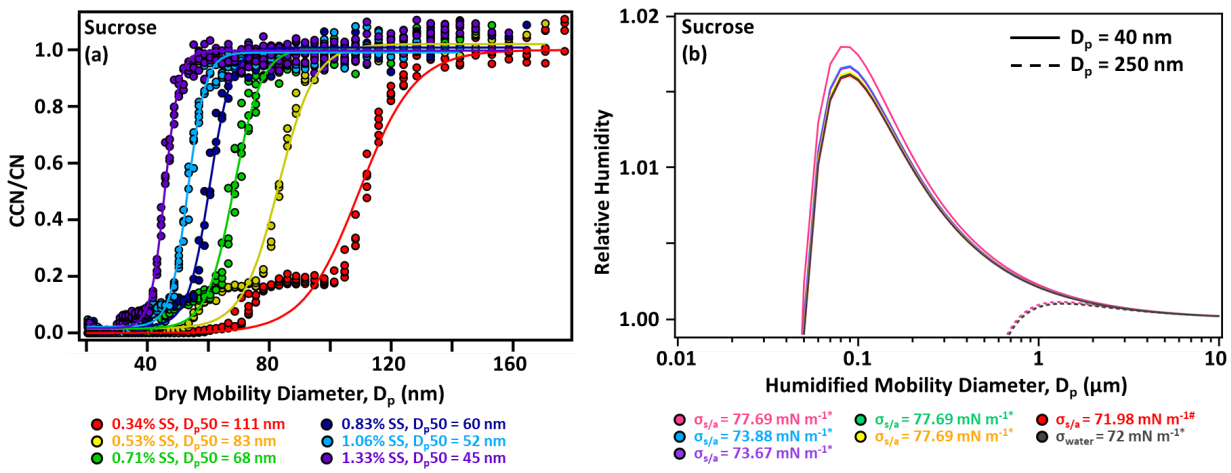

3.4 Comparison of κ-values

Hygroscopicity, (κ_{Ideal}) can be calculated from known solute parameters. Four additional κ-values ($\kappa_{CRD,Mie}$, $\kappa_{CRD,Empirical}$, κ_{HTDMA}, κ_{CCNC}) are calculated from the measurement as data described above. The values of $\kappa_{CRD,Mie}$, and $\kappa_{CRD,Empirical}$ are from converted optical growth factors (Fig. 5). For CRDS-derived κ-values, the error in individual data points is quite high due to fluctuations in relative humidity and particle concentration throughout the experiment. Generally, the highest errors occur for the larger particle sizes where particle concentrations vary the most. The κ factor for each sugar is averaged across all measured particle sizes before the data are interpreted.

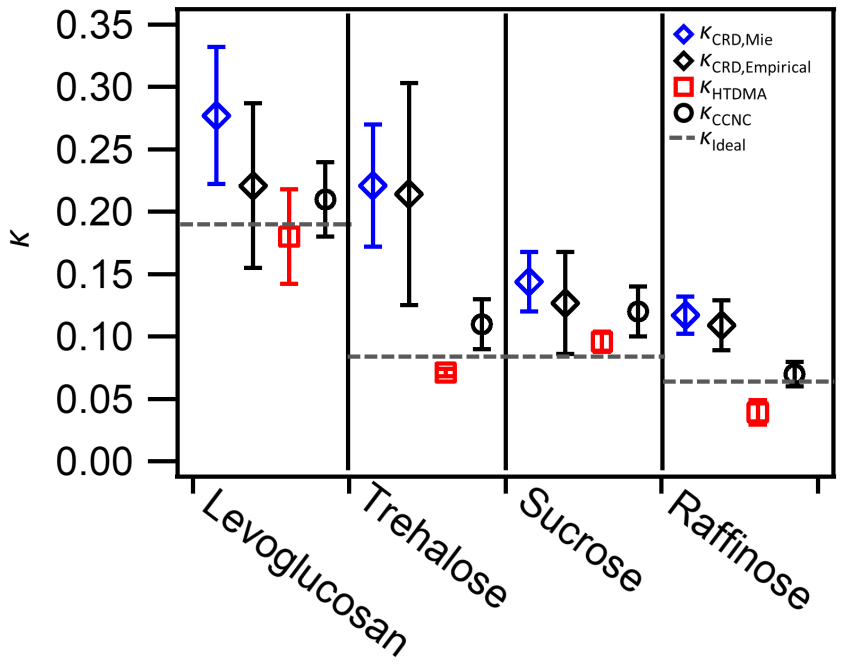

As previously mentioned, the optical growth factor is converted to κ-values using two methods (Section 2.4). Figure 6 provides the first published direct comparison of the two optical growth κ analysis methods for sucrose, raffinose, trehalose, levoglucosan, and $(NH_4)_2SO_4$. Overall, $\kappa_{CRD,Empirical}$ estimates lower values than $\kappa_{CRD,Mie}$ (Fig. 5 and 6). The slope of all the data is 0.83. The empirical model was developed with ammonium sulfate data and is applied to both inorganic and organic *f*RH measurements here. Both $\kappa_{CRD,Empirical}$ and $\kappa_{CRD,Mie}$ values are sensitive to R.H. and larger than κ_{Ideal}. $\kappa_{CRD,Mie}$ is corrected for particle size with Mie theory and thus less dependent on dry particle size (Fig 6b). However, $\kappa_{CRD,Empirical}$ is dependent on dry aerosol particle size. $\kappa_{CRD,Empirical}$ follows the trends in the *f*RH measured data and is more sensitive to initial dry particle size. $\kappa_{CRD,Empirical}$ approaches values of κ_{Ideal} at all sizes with the greatest deviation observed for trehalose. Larger particles are more likely to swell and thus approach the assumptions of dilution that are made by Köhler theory and as applied to κ_{Ideal}. There is a slight deviation between $\kappa_{CRD,Empirical}$ and $\kappa_{CRD,Mie}$ due to each having a slight size dependence, however

within the range of particles sizes in this study $\kappa_{CRD,Empirical}$ serves as a good estimate for $\kappa_{CRD,Mie}$ (Figs. 5 and 6).

Figure SEQ Figure * ARABIC 6: Comparison of single-κ parametrization from *f*RH data. **(a)** κ-values derived from Mie theory and from κ-values from an empirical correlation. All data (black closed circles) is shown for ammonium sulfate, levoglucosan, sucrose, trehalose, and raffinose. The best fit slope (solid red line) = 0.83. Data for ammonium sulfate (red squares), levoglucosan (green triangles), sucrose (blue diamonds), trehalose (purple circles) and raffinose (orange triangles) highlighted. Dashed lines represent 1:1 and 10% uncertainty. **(b)** Size dependence of *f*RH derived κ. Ammonium sulfate (red squares), levoglucosan (green triangles) sucrose (blue diamonds), trehalose (purple circles) and raffinose (orange triangles) are highlighted. Ideal values κ-values are shown (solid lines). $\kappa_{CRD,Mie}$ (open symbols) is size independent and $\kappa_{CRD,Empirical}$ (closed symbols) is size dependent. Both κ-values approach ideal κ-values at larger diameters (> 400 nm).

The *f*RH and G_f data from previous literature were converted into κ-values using Eq. (14) and Eq. (9), respectively. These κ-values are compared with our data for both levoglucosan and sucrose (Fig. 7a and Fig. 7b, Supplemental Information Table S1). In most cases, an online plot digitizer evaluated the mean, minimum, and maximum values for each data point shown in Fig. 7. The minimum and maximum values represent a standard deviation around the mean. The mean *f*RH and G_f values obtained from the literature were then converted to κ-values with the appropriate equation depending on measurement type and the minimum and maximum values were converted into an error for the κ-values. In some cases, information was absent in the

original works that is necessary for a more rigorous error calculation to be performed. In particular, Svenningsson et al.[16], Estillore et al.[26], and Tong et al.[31] did not provide sufficient information for a calculation of error. In the case of Chan et al.[17], nearby points were grouped together and a standard deviation was calculated. Error in the works by Garland et al.[42] and Robinson et al.[43] were determined by using an estimated 3% error associated with the experimental technique. It should be noted that large deviations are not unexpected since the experimental conditions are often quite different from each other. Most notably, the R.H. of the experiments differs by at least five percent in many cases and the dependence of experimentally derived κ-values on uncertain experimental R.H. conditions explains the deviations from theoretically derived values. The R.H. used in the calculation of κ-values for the presented literature is provided in the corresponding sections above by measurement type. Specifically, the κ-values derived from previous CRD literature deviated the most from our work, perhaps because the literature *f*RH experiments were performed at 80% R.H. An additional κ-value derived from Robinson et al.[43] was for raffinose, which was 0.051 ± 0.008 and fits well within the range of κ-values presented in this work. Note that the dry mobility diameter ranges studied in this work are similar to Garland et al. (146 – 627 nm)[42]. Robinson et al. used particles with a mobility diameter of 200 – 500 nm for sucrose and a mobility diameter of 300 nm for raffinose.[43]

κ-values that are determined by CRDS are typically higher than those determined by CCNC, likely due to the influence of the doubly charged particles, which are larger and therefore uptake more water. Doubly charged particles are not accounted for during the *f*RH analysis. Conversely, κ_{HTDMA} values are lower, ranging from 0.039 to 0.180 due to high R.H. (95%) in that system and the sensitivity of κ values to R.H. Overall, the κ-values decrease with an increase in the molecular weight of the organic compound. The coefficient of determination between the

four κ values and the molecular weights range from 0.62-0.95 (Supplemental Information Table S1). According to Köhler theory, this result is expected, but notably, there does not appear to be a trend with the O:C ratio within the limited range of O:C values used in this work. The coefficient of determination between the four κ values and the O:C ratios range from 0.17-0.57. Likewise, the relationship between the κ values and the solubilities is weak with coefficients ranging from 0.02-0.15 (Supplemental Information Table S2). Sparingly soluble organics with solubilities above 100 g L^{-1} are assumed to fully dissolve and readily uptake water[11,65]. The work of Riipinen at al[11] suggests that solubility between 0.1 to 100 g L^{-1} may have observable effects on water-uptake. Furthermore, Petters & Kreidenweis[65] determined that if the volume of compound per unit volume of water is between 0.2 and 0.0005 solubility effects can occur. The effects of limited solubility for raffinose and levoglucosan are calculated in Supplemental Figure S6. Limited solubility calculations indicate levoglucosan and raffinose require critical supersaturations above simple Köhler predictions. However observational results are close to that of ideal fully deliquesced aerosol (Figure 5). The derived experimental hygroscopicity values at sub- and supersaturated conditions suggest that the aerosol is fully deliquesced. The κ-value uncertainties reported in table 2 are small and indicate that aerosol may (as previously postulated) contain the presence of small amounts of soluble impurities.[68] These data also agree with the conclusions in previous literature that show a dependence of organic particles' physical and hygroscopic properties on molecular weight.[33,69,70] Specifically the work by Koop et al.[33] who showed that the thermal glass transition was dependent upon molecular weight and with Rosenørn et al. .[15] who demonstrated that the CCN activity of various saccharides was dependent on molecular weight.[15,33] These results qualitatively suggest that molecular weight of known

aerosol compounds may play a larger role in κ than the relative abundance of hydroxyl groups for the sugars studied here. .

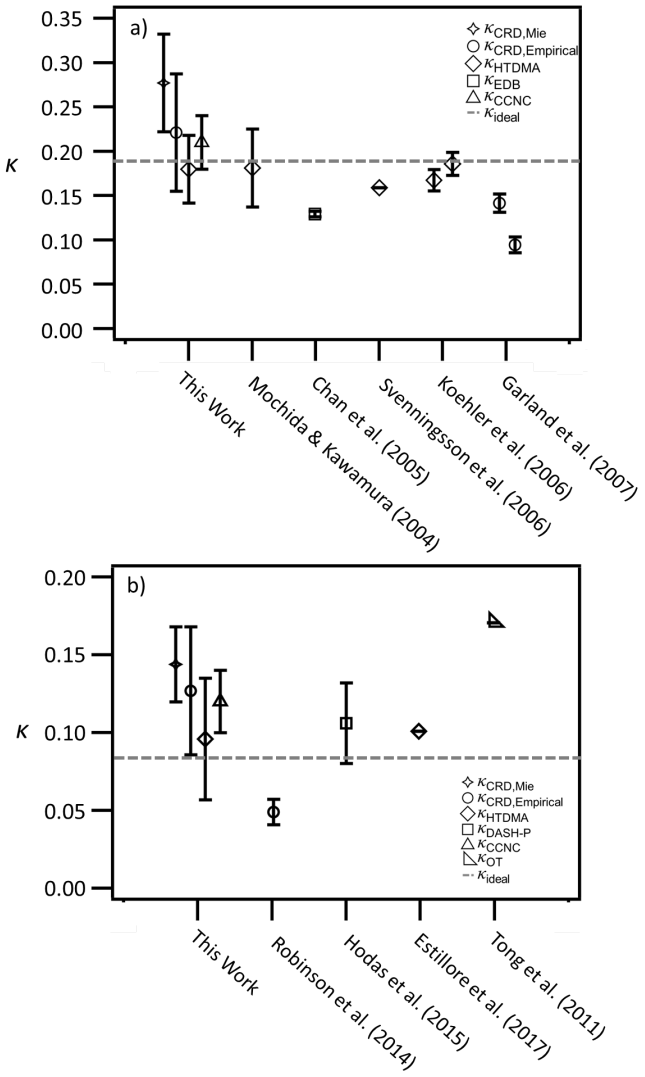

Figure SEQ Figure * ARABIC 7: The κ-values for levoglucosan are compared to values calculated in the literature in a) and the κ-values for sucrose are compared to values calculated in the literature in b). The symbols designate the original measurement type used by the respective authors. Error is derived from those original works. Any points with no error could not be derived, (e.g., Svenningsson et al.[16], Estillore et al.[26], and Tong et al.[31]). The hygroscopicity data in the works of other authors were obtained at various RHs as stated in this text. κ_{OT} represents data collected with optical tweezers (OT).

4. Summary and Implications

This work adds to the growing body of work that measures the droplet growth of WSOCs. To our knowledge, this is the first study that compares these different methods (CRDS, H-TDMA, and CCNC), which is important for comparing subsaturated and supersaturated κ and optical methods to geometric methods for determining subsaturated κ. While H-TDMA and CCNC measurements of water uptake are found in the literature, the use of CRDS for *f*RH measurements is less common. Here we are able to apply a less computationally expensive parameterization to *f*RH ($\kappa_{CRD,Empirical}$), which agrees well with already published methods to obtain κ via the use of Mie theory ($\kappa_{CRD,Mie}$) with good agreement between the two. The *f*RH comparison has been shown to work well for ammonium sulfate, and now here for WSOCs with varying molecular weight measured at higher R.H. The validity of the application of Köhler theory to subsaturated aerosol particles was considered due to the common assumptions used in

the calculation of κ value. Specifically, the surface tension of a sucrose-water solution was measured at varying concentrations and applied to the calculation of κ value with no significant variation in the resulting value. Therefore, Köhler theory (assuming a droplet surface tension equal to that of pure water) was applied to both CRDS and H-TDMA measurements. Each of the four determinations of κ presented in this work ($\kappa_{CRD,Mie,}$ $\kappa_{CRD,Empirical,}$ $\kappa_{HTDMA,}$ κ_{CCNC}) shows the same trend; a decrease in κ with increasing molecular weight. This result agrees with findings in previous literature and matches the theoretical predictions derived from Köhler theory. A greater understanding of hygroscopicity of saccharides in the sub- and supersaturated regimes using several common techniques will help us understand the water uptake behavior of non-surface active WSOCs in atmospheric particles.

AUTHOR INFORMATION

Corresponding Authors

Miriam Arak Freedman; email to maf43@psu.edu. Telephone: +1-814-867-4267
Akua Asa-Awuku; email to: asaawuku@umd.edu. Telephone: +1-301-405-8527
Dabrina D Dutcher; email to ddd014@bucknell.edu
Timothy M. Raymond; email to traymond@bucknell.edu

Author Contributions

JND and MAF designed and performed the CRDS experiments. AAA, TMR, DDD, KAM and PNR designed and performed the CCN experiments. AAA, TMR, DDD, MAF, KAM, PNR, and JND designed and performed the H-TDMA experiments. AAA, DDD, KAM and PNR did the analysis and calculations for H-TDMA and CCN data. JND and MAF performed the calculations using the CRDS data. AAA calculated $\kappa_{CRD,Empirical}$ from CRDS data. All authors contributed to writing and preparing the manuscript.

Funding Sources

U.S. National Science Foundation Award (NSF) 1255832, 1723290, 1723874.

ACKNOWLEDGMENT

MAF and JND acknowledge support from the NSF: AGS-1723290, and E.-J. E. Ott for her work on the measurement of sucrose surface tension. JND acknowledges funding from the NSF GRFP (NSF 1255832). AAA and PNR acknowledge support from the NSF: 1723920. DDD, TMR, and KAM acknowledge support from the NSF: 1723874, and thank H. Jacoby for her contributions to the first field campaign, as well as, K. Nguyen, L. Romano and B. King for their software.

Supporting Information

The supplement related to this article is available online. This supplemental document includes the statistical coefficients of determinations between the four κ-values and compound properties, the method of determining relative humidity within the H-TDMA system via an ammonium sulfate standard, the presentation of refractive indices for each of the compounds of interest in this study, the comparison of experimental values obtained by our cavity ring-down system to Mie theory and subsequent demonstration of the fitting procedure using a known standard, an

illustration of the change in surface tension of a sucrose-water solution with varying concentrations of sucrose, and CCN calibration data using a known standard.

REFERENCES

(1) Yu, H.; Kaufman, Y. J.; Chin, M.; Feingold, G.; Remer, L. A.; Anderson, T. L.; Balkanski, Y.; Bellouin, N.; Boucher, O.; Christopher, S.; DeCola, P.; Kahn, R.; Koch, D.; Loeb, N.; Reddy, M. S.; Schulz, M.; Takemura, T.; Zhou, M. A Review of Measurement-Based Assessments of the Aerosol Direct Radiative Effect and Forcing. *Atmospheric Chemistry and Physics*. 2006, pp 613–666. https://doi.org/10.5194/acp-6-613-2006.

(2) Haywood, J.; Boucher, O. Estimates of the Direct and Indirect Radiative Forcing due to Tropospheric Aerosols: A Review. *Reviews of Geophysics*. 2000, pp 513–543. https://doi.org/10.1029/1999rg000078.

(3) Lohmann, U.; Feichter, J. Global Indirect Aerosol Effects: A Review. *Atmospheric Chemistry and Physics Discussions*. 2004, pp 7561–7614. https://doi.org/10.5194/acpd-4-7561-2004.

(4) Kanakidou, M.; Seinfeld, J. H.; Pandis, S. N.; Barnes, I.; Dentener, F. J.; Facchini, M. C.; Van Dingenen, R.; Ervens, B.; Nenes, A.; Nielsen, C. J.; Swietlicki, E.; Putaud, J. P.; Balkanski, Y.; Fuzzi, S.; Horth, J.; Moortgat, G. K.; Winterhalter, R.; Myhre, C. E. L.; Tsigaridis, K.; Vignati, E.; Stephanou, E. G.; Wilson, J. Organic Aerosol and Global Climate Modelling: A Review. *Atmos. Chem. Phys.* **2005**, *5* (4), 1053–1123. https://doi.org/10.5194/acp-5-1053-2005.

(5) Decesari, S.; Facchini, M. C.; Fuzzi, S.; McFiggans, G. B.; Coe, H.; Bower, K. N. The Water-Soluble Organic Component of Size-Segregated Aerosol, Cloud Water and Wet Depositions from Jeju Island during ACE-Asia. *Atmospheric Environment*. 2005, pp 211–222. https://doi.org/10.1016/j.atmosenv.2004.09.049.

(6) Falkovich, A. H.; Graber, E. R.; Schkolnik, G.; Rudich, Y.; Maenhaut, W.; Artaxo, P. Low Molecular Weight Organic Acids in Aerosol Particles from Rondônia, Brazil, during the Biomass-Burning, Transition and Wet Periods. *Atmospheric Chemistry and Physics*. 2005, pp 781–797. https://doi.org/10.5194/acp-5-781-2005.

(7) Graham, B.; Mayol-Bracero, O. L.; Guyon, P.; Roberts, G. C.; Decesari, S.; Facchini, M. C.; Artaxo, P.; Maenhaut, W.; Köll, P.; Andreae, M. O. Water-Soluble Organic Compounds in Biomass Burning Aerosols over Amazonia 1. Characterization by NMR and GC-MS. *J. Geophys. Res. D: Atmos.* **2002**, *107* (D20), LBA – 14.

(8) Schkolnik, G.; Falkovich, A. H.; Rudich, Y.; Maenhaut, W.; Artaxo, P. New Analytical Method for the Determination of Levoglucosan, Polyhydroxy Compounds, and 2-Methylerythritol and Its Application to Smoke and Rainwater Samples. *Environ. Sci. Technol.* **2005**, *39* (8), 2744–2752. https://doi.org/10.1021/es048363c.

(9) Mayol-Bracero, O. L. Water-Soluble Organic Compounds in Biomass Burning Aerosols over Amazonia 2. Apportionment of the Chemical Composition and Importance of the Polyacidic Fraction. *Journal of Geophysical Research*. 2002. https://doi.org/10.1029/2001jd000522.

(10) Chan, M. N.; Kreidenweis, S. M.; Chan, C. K. Measurements of the Hygroscopic and Deliquescence Properties of Organic Compounds of Different Solubilities in Water and Their Relationship with Cloud Condensation Nuclei Activities. *Environ. Sci. Technol.* **2008**, *42* (10), 3602–3608. https://doi.org/10.1021/es7023252.

(11) Riipinen, I.; Rastak, N.; Pandis, S. N. Connecting the Solubility and CCN Activation of Complex Organic Aerosols: A Theoretical Study Using Solubility Distributions. *Atmospheric Chemistry and Physics*. 2015, pp 6305–6322.

https://doi.org/10.5194/acp-15-6305-2015.
(12) Gao, S.; Hegg, D. A.; Hobbs, P. V.; Kirchstetter, T. W.; Magi, B. I.; Sadilek, M. Water-Soluble Organic Components in Aerosols Associated with Savanna Fires in Southern Africa: Identification, Evolution, and Distribution. *Journal of Geophysical Research: Atmospheres*. 2003. https://doi.org/10.1029/2002jd002324.
(13) Schkolnik, G.; Rudich, Y. Detection and Quantification of Levoglucosan in Atmospheric Aerosols: A Review. *Anal. Bioanal. Chem.* **2006**, *385* (1), 26–33. https://doi.org/10.1007/s00216-005-0168-5.
(14) Simoneit, B. R. T.; Schauer, J. J.; Nolte, C. G.; Oros, D. R.; Elias, V. O.; Fraser, M. P.; Rogge, W. F.; Cass, G. R. Levoglucosan, a Tracer for Cellulose in Biomass Burning and Atmospheric Particles. *Atmospheric Environment*. 1999, pp 173–182. https://doi.org/10.1016/s1352-2310(98)00145-9.
(15) Rosenorn, T.; Kiss, G.; Bilde, M. Cloud Droplet Activation of Saccharides and Levoglucosan Particles. *Atmospheric Environment*. 2006, pp 1794–1802. https://doi.org/10.1016/j.atmosenv.2005.11.024.
(16) Svenningsson, B.; Rissler, J.; Swietlicki, E.; Mircea, M.; Bilde, M.; Facchini, M. C.; Decesari, S.; Fuzzi, S.; Zhou, J.; Mønster, J.; Rosenørn, T. Hygroscopic Growth and Critical Supersaturations for Mixed Aerosol Particles of Inorganic and Organic Compounds of Atmospheric Relevance. *Atmospheric Chemistry and Physics*. 2006, pp 1937–1952. https://doi.org/10.5194/acp-6-1937-2006.
(17) Chan, M. N.; Choi, M. Y.; Ng, N. L.; Chan, C. K. Hygroscopicity of Water-Soluble Organic Compounds in Atmospheric Aerosols: Amino Acids and Biomass Burning Derived Organic Species. *Environ. Sci. Technol.* **2005**, *39* (6), 1555–1562. https://doi.org/10.1021/es049584l.
(18) Lienhard, D. M.; Bones, D. L.; Zuend, A.; Krieger, U. K.; Reid, J. P.; Peter, T. Measurements of Thermodynamic and Optical Properties of Selected Aqueous Organic and Organic-Inorganic Mixtures of Atmospheric Relevance. *J. Phys. Chem. A* **2012**, *116* (40), 9954–9968. https://doi.org/10.1021/jp3055872.
(19) Lei, T.; Zuend, A.; Wang, W. G.; Zhang, Y. H.; Ge, M. F. Hygroscopicity of Organic Compounds from Biomass Burning and Their Influence on the Water Uptake of Mixed Organic Ammonium Sulfate Aerosols. *Atmospheric Chemistry and Physics*. 2014, pp 11165–11183. https://doi.org/10.5194/acp-14-11165-2014.
(20) Mochida, M.; Kawamura, K. Hygroscopic Properties of Levoglucosan and Related Organic Compounds Characteristic to Biomass Burning Aerosol Particles. *Journal of Geophysical Research: Atmospheres*. 2004. https://doi.org/10.1029/2004jd004962.
(21) Decesari, S.; Fuzzi, S.; Facchini, M. C.; Mircea, M.; Emblico, L.; Cavalli, F.; Maenhaut, W.; Chi, X.; Schkolnik, G.; Falkovich, A.; Rudich, Y.; Claeys, M.; Pashynska, V.; Vas, G.; Kourtchev, I.; Vermeylen, R.; Hoffer, A.; Andreae, M. O.; Tagliavini, E.; Moretti, F.; Artaxo, P. Characterization of the Organic Composition of Aerosols from Rondônia, Brazil, during the LBA-SMOCC 2002 Experiment and Its Representation through Model Compounds. *Atmospheric Chemistry and Physics Discussions*. 2005, pp 5687–5749. https://doi.org/10.5194/acpd-5-5687-2005.
(22) Pashynska, V.; Vermeylen, R.; Vas, G.; Maenhaut, W.; Claeys, M. Development of a Gas Chromatographic/ion Trap Mass Spectrometric Method for the Determination of Levoglucosan and Saccharidic Compounds in Atmospheric Aerosols. Application to Urban Aerosols. *J. Mass Spectrom.* **2002**, *37* (12), 1249–1257. https://doi.org/10.1002/jms.391.
(23) Yttri, K. E.; Dye, C.; Kiss, G. Ambient Aerosol Concentrations of Sugars and

Sugar-Alcohols at Four Different Sites in Norway. *Atmospheric Chemistry and Physics Discussions*. 2007, pp 5769–5803. https://doi.org/10.5194/acpd-7-5769-2007.
(24) Chenyakin, Y.; Ullmann, D. A.; Evoy, E.; Renbaum-Wolff, L.; Kamal, S.; Bertram, A. K. Diffusion Coefficients of Organic Molecules in Sucrose–water Solutions and Comparison with Stokes–Einstein Predictions. *Atmospheric Chemistry and Physics*. 2017, pp 2423–2435. https://doi.org/10.5194/acp-17-2423-2017.
(25) Ekdawi-Sever, N.; de Pablo, J. J.; Feick, E.; von Meerwall, E. Diffusion of Sucrose and α,α-Trehalose in Aqueous Solutions. *The Journal of Physical Chemistry A*. 2003, pp 936–943. https://doi.org/10.1021/jp020187b.
(26) Estillore, A. D.; Morris, H. S.; Or, V. W.; Lee, H. D.; Alves, M. R.; Marciano, M. A.; Laskina, O.; Qin, Z.; Tivanski, A. V.; Grassian, V. H. Linking Hygroscopicity and the Surface Microstructure of Model Inorganic Salts, Simple and Complex Carbohydrates, and Authentic Sea Spray Aerosol Particles. *Phys. Chem. Chem. Phys.* **2017**, *19* (31), 21101–21111. https://doi.org/10.1039/c7cp04051b.
(27) Hodas, N.; Zuend, A.; Mui, W.; Flagan, R. C.; Seinfeld, J. H. Influence of Particle-Phase State on the Hygroscopic Behavior of Mixed Organic–inorganic Aerosols. *Atmospheric Chemistry and Physics*. 2015, pp 5027–5045. https://doi.org/10.5194/acp-15-5027-2015.
(28) Marshall, F. H.; Miles, R. E. H.; Song, Y.-C.; Ohm, P. B.; Power, R. M.; Reid, J. P.; Dutcher, C. S. Diffusion and Reactivity in Ultraviscous Aerosol and the Correlation with Particle Viscosity. *Chem. Sci.* **2016**, *7* (2), 1298–1308. https://doi.org/10.1039/c5sc03223g.
(29) Power, R. M.; Simpson, S. H.; Reid, J. P.; Hudson, A. J. The Transition from Liquid to Solid-like Behaviour in Ultrahigh Viscosity Aerosol Particles. *Chemical Science*. 2013, p 2597. https://doi.org/10.1039/c3sc50682g.
(30) Rothfuss, N. E.; Marsh, A.; Rovelli, G.; Petters, M. D.; Reid, J. P. Condensation Kinetics of Water on Amorphous Aerosol Particles. *The Journal of Physical Chemistry Letters*. 2018, pp 3708–3713. https://doi.org/10.1021/acs.jpclett.8b01365.
(31) Tong, H.-J.; Reid, J. P.; Bones, D. L.; Luo, B. P.; Krieger, U. K. Measurements of the Timescales for the Mass Transfer of Water in Glassy Aerosol at Low Relative Humidity and Ambient Temperature. *Atmospheric Chemistry and Physics*. 2011, pp 4739–4754. https://doi.org/10.5194/acp-11-4739-2011.
(32) Zobrist, B.; Soonsin, V.; Luo, B. P.; Krieger, U. K.; Marcolli, C.; Peter, T.; Koop, T. Ultra-Slow Water Diffusion in Aqueous Sucrose Glasses. *Phys. Chem. Chem. Phys.* **2011**, *13* (8), 3514–3526. https://doi.org/10.1039/c0cp01273d.
(33) Koop, T.; Bookhold, J.; Shiraiwa, M.; Pöschl, U. Glass Transition and Phase State of Organic Compounds: Dependency on Molecular Properties and Implications for Secondary Organic Aerosols in the Atmosphere. *Phys. Chem. Chem. Phys.* **2011**, *13* (43), 19238–19255. https://doi.org/10.1039/c1cp22617g.
(34) Lee, H. D.; Ray, K. K.; Tivanski, A. V. Directly Probing the Phase States and Surface Tension of Individual Submicrometer Particles Using Atomic Force Microscopy. In *Multiphase Environmental Chemistry in the Atmosphere*; Hunt, S. W., Laskin, A., Nizkorodov, S. A., Eds.; American Chemical Society, Series Ed.; ACS Symposium Series; American Chemical Society: Washington, DC, 2018; Vol. 1299, pp 245–259. https://doi.org/10.1021/bk-2018-1299.ch012.
(35) Müller, A.; Miyazaki, Y.; Tachibana, E.; Kawamura, K.; Hiura, T. Evidence of a Reduction in Cloud Condensation Nuclei Activity of Water-Soluble Aerosols Caused by Biogenic Emissions in a Cool-Temperate Forest. *Scientific Reports*. 2017.

https://doi.org/10.1038/s41598-017-08112-9.
(36) Rogge, W. F.; Medeiros, P. M.; Simoneit, B. R. T. Organic Marker Compounds in Surface Soils of Crop Fields from the San Joaquin Valley Fugitive Dust Characterization Study. *Atmospheric Environment*. 2007, pp 8183–8204. https://doi.org/10.1016/j.atmosenv.2007.06.030.
(37) Tang, M.; Chan, C. K.; Li, Y. J.; Su, H.; Ma, Q.; Wu, Z.; Zhang, G.; Wang, Z.; Ge, M.; Hu, M.; He, H.; Wang, X. A Review of Experimental Techniques for Aerosol Hygroscopicity Studies. *Atmospheric Chemistry and Physics*. 2019, pp 12631–12686. https://doi.org/10.5194/acp-19-12631-2019.
(38) Baynard, T.; Garland, R. M.; Ravishankara, A. R.; Tolbert, M. A.; Lovejoy, E. R. Key Factors Influencing the Relative Humidity Dependence of Aerosol Light Scattering. *Geophysical Research Letters*. 2006. https://doi.org/10.1029/2005gl024898.
(39) Beaver, M. R.; Baynard, T.; Garland, R. M.; Hasenkopf, C.; Ravishankara, A. R.; Tolbert, M. A. Relative Humidity Dependence of Light Extinction by Mixed Organic/Sulfate Particles. *Nucleation and Atmospheric Aerosols*. 2007, pp 916–919. https://doi.org/10.1007/978-1-4020-6475-3_180.
(40) Cappa, C. D.; Che, D. L.; Kessler, S. H.; Kroll, J. H.; Wilson, K. R. Variations in Organic Aerosol Optical and Hygroscopic Properties upon Heterogeneous OH Oxidation. *Journal of Geophysical Research*. 2011. https://doi.org/10.1029/2011jd015918.
(41) Flores, J. M.; Michel Flores, J.; Bar-Or, R. Z.; Bluvshtein, N.; Abo-Riziq, A.; Kostinski, A.; Borrmann, S.; Koren, I.; Koren, I.; Rudich, Y. Absorbing Aerosols at High Relative Humidity: Linking Hygroscopic Growth to Optical Properties. *Atmospheric Chemistry and Physics*. 2012, pp 5511–5521. https://doi.org/10.5194/acp-12-5511-2012.
(42) Garland, R. M.; Ravishankara, A. R.; Lovejoy, E. R.; Tolbert, M. A.; Baynard, T. Parameterization for the Relative Humidity Dependence of Light Extinction: Organic-Ammonium Sulfate Aerosol. *Journal of Geophysical Research*. 2007. https://doi.org/10.1029/2006jd008179.
(43) Robinson, C. B.; Schill, G. P.; Tolbert, M. A. Optical Growth of Highly Viscous Organic/sulfate Particles. *Journal of Atmospheric Chemistry*. 2014, pp 145–156. https://doi.org/10.1007/s10874-014-9287-8.
(44) Brown, S. S.; Stark, H.; Ravishankara, A. R. Cavity Ring-down Spectroscopy for Atmospheric Trace Gas Detection: Application to the Nitrate Radical (NO_3). *Applied Physics B: Lasers and Optics*. 2002, pp 173–182. https://doi.org/10.1007/s00340-002-0980-y.
(45) Wex, H.; Petters, M. D.; Carrico, C. M.; Hallbauer, E.; Massling, A.; McMeeking, G. R.; Poulain, L.; Wu, Z.; Kreidenweis, S. M.; Stratmann, F. Towards Closing the Gap between Hygroscopic Growth and Activation for Secondary Organic Aerosol: Part 1 – Evidence from Measurements. *Atmospheric Chemistry and Physics*. 2009, pp 3987–3997. https://doi.org/10.5194/acp-9-3987-2009.
(46) Petters, M. D.; Kreidenweis, S. M. A Single Parameter Representation of Hygroscopic Growth and Cloud Condensation Nucleus Activity. *Atmospheric Chemistry and Physics*. 2007, pp 1961–1971. https://doi.org/10.5194/acp-7-1961-2007.
(47) Altaf, M. B.; Freedman, M. A. Effect of Drying Rate on Aerosol Particle Morphology. *The Journal of Physical Chemistry Letters*. 2017, pp 3613–3618. https://doi.org/10.1021/acs.jpclett.7b01327.
(48) Veghte, D. P.; Freedman, M. A. The Necessity of Microscopy to Characterize the Optical

Properties of Size-Selected, Nonspherical Aerosol Particles. *Analytical Chemistry*. 2012, pp 9101–9108. https://doi.org/10.1021/ac3017373.
(49) Veghte, D. P.; Freedman, M. A. Facile Method for Determining the Aspect Ratios of Mineral Dust Aerosol by Electron Microscopy. *Aerosol Science and Technology*. 2014, pp 715–724. https://doi.org/10.1080/02786826.2014.920484.
(50) Veghte, D. P.; Altaf, M. B.; Haines, J. D.; Freedman, M. A. Optical Properties of Non-Absorbing Mineral Dust Components and Mixtures. *Aerosol Science and Technology*. 2016, pp 1239–1252. https://doi.org/10.1080/02786826.2016.1225153.
(51) Pettersson, A.; Lovejoy, E. R.; Brock, C. A.; Brown, S. S.; Ravishankara, A. R. Measurement of Aerosol Optical Extinction at with Pulsed Cavity Ring down Spectroscopy. *Journal of Aerosol Science*. 2004, pp 995–1011. https://doi.org/10.1016/j.jaerosci.2004.02.008.
(52) Freedman, M. A.; Hasenkopf, C. A.; Beaver, M. R.; Tolbert, M. A. Optical Properties of Internally Mixed Aerosol Particles Composed of Dicarboxylic Acids and Ammonium Sulfate. *The Journal of Physical Chemistry A*. 2009, pp 13584–13592. https://doi.org/10.1021/jp906240y.
(53) Hasenkopf, C. A.; Beaver, M. R.; Trainer, M. G.; Langley Dewitt, H.; Freedman, M. A.; Toon, O. B.; McKay, C. P.; Tolbert, M. A. Optical Properties of Titan and Early Earth Haze Laboratory Analogs in the Mid-Visible. *Icarus*. 2010, pp 903–913. https://doi.org/10.1016/j.icarus.2009.12.015.
(54) Cruz, C. N.; Pandis, S. N. Deliquescence and Hygroscopic Growth of Mixed Inorganic−Organic Atmospheric Aerosol. *Environmental Science & Technology*. 2000, pp 4313–4319. https://doi.org/10.1021/es9907109.
(55) Rader, D. J.; McMurry, P. H. Application of the Tandem Differential Mobility Analyzer to Studies of Droplet Growth or Evaporation. *Journal of Aerosol Science*. 1986, pp 771–787. https://doi.org/10.1016/0021-8502(86)90031-5.
(56) Swietlicki, E.; Hansson, H.-C.; Hämeri, K.; Svenningsson, B.; Massling, A.; Mcfiggans, G.; Mcmurry, P. H.; Petäjä, T.; Tunved, P.; Gysel, M.; Topping, D.; Weingartner, E.; Baltensperger, U.; Rissler, J.; Wiedensohler, A.; Kulmala, M. Hygroscopic Properties of Submicrometer Atmospheric Aerosol Particles Measured with H-TDMA Instruments in Various Environments—a Review. *Tellus B: Chemical and Physical Meteorology*. 2008, pp 432–469. https://doi.org/10.1111/j.1600-0889.2008.00350.x.
(57) Taylor, N. F.; Collins, D. R.; Spencer, C. W.; Lowenthal, D. H.; Zielinska, B.; Samburova, V.; Kumar, N. Measurement of Ambient Aerosol Hydration State at Great Smoky Mountains National Park in the Southeastern United States. *Atmospheric Chemistry and Physics*. 2011, pp 12085–12107. https://doi.org/10.5194/acp-11-12085-2011.
(58) Moore, R. H.; Nenes, A.; Medina, J. Scanning Mobility CCN Analysis—A Method for Fast Measurements of Size-Resolved CCN Distributions and Activation Kinetics. *Aerosol Science and Technology*. 2010, pp 861–871. https://doi.org/10.1080/02786826.2010.498715.
(59) Rose, D.; Gunthe, S. S.; Mikhailov, E.; Frank, G. P.; Dusek, U.; Andreae, M. O.; Pöschl, U. Calibration and Measurement Uncertainties of a Continuous-Flow Cloud Condensation Nuclei Counter (DMT-CCNC): CCN Activation of Ammonium Sulfate and Sodium Chloride Aerosol Particles in Theory and Experiment. *Atmospheric Chemistry and Physics*. 2008, pp 1153–1179. https://doi.org/10.5194/acp-8-1153-2008.
(60) Clegg, S. L.; Wexler, A. S.; Brimblecombe, P. Properties of Acid Ammonium Sulphate

Aerosols at Low Temperature. *Journal of Aerosol Science*. 1998, pp S535–S536. https://doi.org/10.1016/s0021-8502(98)00243-2.
(61) Suda, S. R.; Petters, M. D. Accurate Determination of Aerosol Activity Coefficients at Relative Humidities up to 99% Using the Hygroscopicity Tandem Differential Mobility Analyzer Technique. *Aerosol Sci. Technol.* **2013**, *47* (9), 991–1000. https://doi.org/10.1080/02786826.2013.807906.
(62) Mikhailov, E. F.; Vlasenko, S. S. High-Humidity Tandem Differential Mobility Analyzer for Accurate Determination of Aerosol Hygroscopic Growth, Microstructure, and Activity Coefficients over a Wide Range of Relative Humidity, 2020. https://doi.org/10.5194/amt-13-2035-2020.
(63) Wang, S. C.; Flagan, R. C. Scanning Electrical Mobility Spectrometer. *Aerosol Science and Technology*. 1990, pp 230–240. https://doi.org/10.1080/02786829008959441.
(64) Kreidenweis, S. M.; Asa-Awuku, A. Aerosol Hygroscopicity: Particle Water Content and Its Role in Atmospheric Processes. *Treatise on Geochemistry*. 2014, pp 331–361. https://doi.org/10.1016/b978-0-08-095975-7.00418-6.
(65) Petters, M. D.; Kreidenweis, S. M. A Single Parameter Representation of Hygroscopic Growth and Cloud Condensation Nucleus Activity – Part 2: Including Solubility. *Atmospheric Chemistry and Physics*. 2008, pp 6273–6279. https://doi.org/10.5194/acp-8-6273-2008.
(66) Lavallard, P.; Rosenbauer, M.; Gacoin, T. Influence of Surrounding Dielectrics on the Spontaneous Emission of sulforhodamineBmolecules. *Physical Review A*. 1996, pp 5450–5453. https://doi.org/10.1103/physreva.54.5450.
(67) Koehler, K. A.; Kreidenweis, S. M.; DeMott, P. J.; Prenni, A. J.; Carrico, C. M.; Ervens, B.; Feingold, G. Water Activity and Activation Diameters from Hygroscopicity Data - Part II: Application to Organic Species. *Atmospheric Chemistry and Physics*. 2006, pp 795–809. https://doi.org/10.5194/acp-6-795-2006.
(68) Bilde, M.; Svenningsson, B. CCN Activation of Slightly Soluble Organics: The Importance of Small Amounts of Inorganic Salt and Particle Phase. *Tellus B*. 2004, pp 128–134. https://doi.org/10.1111/j.1600-0889.2004.00090.x.
(69) Petters, M. D.; Kreidenweis, S. M.; Prenni, A. J.; Sullivan, R. C.; Carrico, C. M.; Koehler, K. A.; Ziemann, P. J. Role of Molecular Size in Cloud Droplet Activation. *Geophys. Res. Lett.* **2009**, *36* (22), 13. https://doi.org/10.1029/2009GL040131.
(70) Wang, J.; Shilling, J. E.; Liu, J.; Zelenyuk, A.; Bell, D. M.; Petters, M. D.; Thalman, R.; Mei, F.; Zaveri, R. A.; Zheng, G. Cloud Droplet Activation of Secondary Organic Aerosol Is Mainly Controlled by Molecular Weight, Not Water Solubility, 2019. https://doi.org/10.5194/acp-19-941-2019.

TOC Graphic

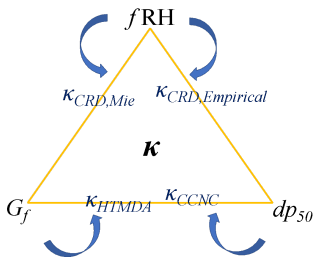
fRH
$\kappa_{CRD,Mie}$
$\kappa_{CRD,Empirical}$
κ
G_f
κ_{HTMDA}
κ_{CCNC}
dp_{50}